Quantifying the Impact of CACC penetration on Phantom Traffic Jam Formation: A Density-Preserving Multi-Lane Study

Aashish Harishchandre
Michigan State University
Department of Computer Science
East Lansing, MI 48824
Email: harishch@msu.edu

Lucas Wolstencroft
Michigan State University
Department of Electrical Engineering
East Lansing, MI 48824
Email: wolstenc@msu.edu

Prabhaav Ravikumar Pillai
Michigan State University
Department of Computer Science
East Lansing, MI 48824
Email: prabhaav@msu.edu

***Abstract*—Phantom traffic jams, stop-and-go waves without any physical bottleneck, impose billions of dollars of annual economic cost on the U.S. transportation system. Cooperative Adaptive Cruise Control (CACC), a vehicle-to-vehicle (V2V) coordination technology that can be deployed with current hardware, offers a near-term mitigation strategy. However, the penetration rate at which CACC begins to deliver measurable improvements in mixed human-AV traffic, and how this threshold shifts in realistic multi-lane road environments, remain open questions with direct policy implications. This paper presents a density-preserving micro-simulation study that sweeps CACC penetration from 0% to 100% across one-, two-, three-, and four-lane ring-road configurations. Three independent seed runs per configuration mitigate AV-placement bias. Results show that meaningful phantom-jam suppression emerges at 40%–60% CACC penetration regardless of lane count. Lane switching provides 20%–24% congestion reduction at low penetration but becomes counterproductive to flow stability above 80%–90% CACC, a finding explained by the MOBIL lane-change incentive criterion persisting even when longitudinal coordination alone has stabilized the flow.**

***Index Terms*—Cooperative Adaptive Cruise Control, phantom traffic jam, mixed traffic, IDM, MOBIL, ring road**

I. Introduction

A. Motivation

Phantom traffic jams, spontaneous stop-and-go waves that form without any physical bottleneck, such as an on-ramp or lane drop, are a well-documented phenomenon [32]. They occur due to small disturbances in driver behavior, such as slight changes in speed or following distance. These disturbances are amplified over time due to human drivers' overreaction. Sugiyama et al. demonstrated experimentally that, even in the absence of external influences, natural fluctuations in driver behavior on a closed ring road are sufficient to produce self-sustaining traffic waves [32]. Stern et al. confirmed that a single autonomous vehicle strategically smoothing its acceleration can partially suppress such waves in a live field experiment [33]. As each driver reacts to the vehicle ahead's behavior, minor fluctuations can grow into significant slowdowns.

The economic significance of phantom jams is substantial; traffic congestion costs the United States approximately $166 billion per year in wasted fuel and lost productivity [34]. The U.S. Department of Transportation has identified the precise CACC penetration thresholds at which CACC systems begin to measurably improve flow as a critical input for planning V2X roadside unit deployments and formulating AV adoption incentive policies [8]. Without quantitative penetration thresholds, infrastructure investments cannot be properly timed or sized.

A roadway composed entirely of autonomous vehicles could theoretically eliminate such traffic jams [5]. However, for the foreseeable future, roads will feature a mix of AVs and human drivers [6]. This mixed-traffic regime is the critical near-term scenario: systems must be designed to deliver benefit at partial adoption levels, not only at full autonomy [7]. This raises the question: what level of CACC-capable vehicle penetration is required to meaningfully mitigate traffic disruptions caused by human driving behavior, and how does the answer change in multi-lane environments?

B. Prior Art

Prior research has established that connected vehicle technologies can improve the performance of mixed-traffic systems [6]–[8], [27]. Gu'eriau and Dusparic (2020) quantify the impact of connected and autonomous vehicles on traffic efficiency and safety in mixed traffic, demonstrating improvements even at partial penetration rates [6]; their work highlights the importance of studying mixed-traffic scenarios rather than comparing purely human-driven vs. fully autonomous roadways, as the transitional mixed regime is the critical near-term reality.

Shladover et al. (2012) conducted a foundational simulation study showing that CACC begins to produce measurable capacity benefits at approximately 50% penetration, but scoped their analysis to a single-lane freeway [8]. Song et al. (2022) developed a data-driven CACC framework for mixed-heterogeneous vehicle platoons with unknown vehicle dynamics enabling CACC-capable vehicles to maintain string

stability against varying leader behaviors [2]. Wang et al. (2022) extended cooperative control to platoon lane-changing, demonstrating that CACC can improve mobility in multi-lane traffic [3]. Molnar and Orosz (2024) showed analytically that increasing the penetration of connected automated vehicles destroys the bistable behavior that gives rise to phantom traffic jams [5]. Milanés et al. (2014) demonstrated CACC in real traffic situations on a highway testbed, validating the string-stability benefits of reduced time headways [27]. Lioris et al. (2017) showed that connected vehicle platoons can nearly double throughput on urban corridors [26]. Their framework enables CACC-capable vehicles to observe patterns in surrounding vehicles and predict their movements, helping maintain string stability.

Alternative shock-wave mitigation strategies, including variable speed limits (VSL) [29]–[31] and model-predictive roadside controllers [30], require fixed infrastructure investments and are less effective on roads with inadequate sensor coverage. V2X-based cooperative control [28] offers an infrastructure-light complement by leveraging onboard V2V communication, motivating the CACC approach studied here.

Most prior microsimulation studies of CACC penetration effects, however, use single-lane ring roads or fix the total number of vehicles as the lane count increases, which effectively reduces density and conflates the benefits of lateral bypass with those of a less congested road [9], [24]. Building on prior work, the present study seeks to address this gap by sweeping penetration rates across $1-4$ lane configurations while holding vehicle density constant at $\sim$44.2 veh/km per lane.

The remainder of this paper is organized as follows: Section II presents the simulation platform, vehicle dynamics models, and experimental design. Section III reports single-lane and multi-lane results across all configurations. Section IV draws conclusions and policy implications.

II. Methodology

A. Simulation Platform and Justification

Several microscopic traffic simulation platforms were evaluated: SUMO (Simulation of Urban Mobility), VISSIM, CARLA/Flow (a reinforcement-learning framework), and traffic-simulation-de (the open-source JavaScript microsimulator by Martin Treiber [19]).

Traffic-simulation-de was selected for three reasons. First, it is the reference implementation of the Intelligent Driver Model (IDM) written by IDM's original author [22], eliminating a model-translation layer that would be present if IDM were re-implemented inside SUMO. SUMO's IDM implementation may have subtle differences in edge-case handling (e.g., the bounded reformulation for cut-in scenarios), whereas traffic-simulation-de's implementation has been used directly in Treiber's published work. Second, the simulator provides native ring-road support with no boundary conditions to model, which is the ideal topology for phantom-jam experiments following Sugiyama et al. [32]. Third, the HTML/JavaScript architecture allows 25 (can be modified as computation permits) headless browser instances to execute concurrently via Python Playwright, enabling the 132-scenario sweep (3 seeds $\times$ 11 penetration rates $\times$ 4 lane counts) in a single run. Although not a specific reason for selection, a strong suit of Traffic-simulation-de is its ability to be visualized and interacted with inside any modern web browser, with no additional installations or dependencies.

Accuracy IDM was originally parameterized and validated against real freeway trajectory data by Treiber and collaborators [22]; the values adopted in this study (Table I) are consistent with those established ranges. MOBIL was validated against German Autobahn lane change field data by Kesting et al. [1]. As a baseline calibration check, the 0% CACC scenario reproduces the qualitative wave dynamics of the Sugiyama et al. physical experiment, persistent backward-propagating stop-and-go bands circulating at approximately -1.2 m/s, consistent with empirical observations [32]. The 0% CACC equilibrium speed of 9.1 m/s at a density of 44.2 veh/km is physically consistent with IDM's fundamental diagram at these parameter values [33].

Although the original simulator supports multiple roadway scenarios and adjustable traffic parameters, this study focused on a single scenario to evaluate the effects of mixed traffic comprising both human-driven and CACC-equipped vehicles. Vehicles in the simulation were assigned as either "conventional" or "CACC-equipped" according to a specified proportion. The behavior of the CACC-equipped vehicles was then modified to incorporate cooperative car-following logic, enabling them to respond differently from conventional vehicles.

B. Longitudinal Dynamics: Intelligent Driver Model

All vehicles follow the Intelligent Driver Model (IDM) [22]:

$$a = a_{\max}\left[1-\left(\frac{v}{v_0}\right)^{\delta}-\left(\frac{s^*(v,\Delta v)}{s}\right)^2\right] \tag{1}$$

$$s^*(v,\Delta v) = s_0 + vT + \frac{v\Delta v}{2\sqrt{a_{\max}\,b}} \tag{2}$$

where v is the ego vehicle speed, v_0 the desired speed, s the current gap to the leader, $\Delta v = v - v_{\text{lead}}$ the approach rate, s^* the desired safety gap, T the time headway, s_0 the minimum stationary gap, $a_{\max}$ maximum acceleration, b comfortable deceleration, and $\delta = 4$ the acceleration exponent. Table I summarizes parameter values used for human-driven vehicles (HV) and CACC-equipped vehicles (AV).

The reduced time headway $T = 0.6$ s for CACC vehicles (vs. $T = 1.4$ s for human drivers) is the key parameter enabling string stability. By maintaining a tighter gap, CACC vehicles can absorb deceleration pulses before they amplify into shock waves; a feedforward term derived from V2V leader-acceleration data further reduces the phase lag inherent in human reaction time [4], [16]:

where $\alpha = 0.5$ is the feedforward gain. This cooperative look-ahead prevents CACC vehicles from being surprised by a braking leader, thereby reducing the amplitude of shockwaves propagating backward through the platoon [10], [16].

TABLE I
IDM PARAMETER VALUES FOR HUMAN DRIVERS (HV) AND CACC VEHICLES (AV)

Parameter	HV	AV (CACC)
v_0 (desired speed)	30 m/s	30 m/s
T (time headway)	1.4 s	**0.6 s**
s_0 (min. gap)	2 m	2 m
$a_{\max}$	1.5 m/s^2	2.0 m/s^2
b (comfort decel.)	2.0 m/s^2	3.0 m/s^2
δ (accel. exponent)	4	4

Algorithm 1 CACC Car-Following Logic

Require: ego vehicle v, immediate leader ℓ, broadcast leader ℓ_b (V2V)
if v.isAV **and** $\ell_b \neq \emptyset$ **then**
  $a_{\text{IDM}} \leftarrow \text{IDM}(v, \ell,\ T = T_{\text{platoon}} = 0.6\ \text{s})$
  $a_{\text{ff}} \leftarrow \alpha \cdot \ell_b.\text{acceleration}$
  $a \leftarrow a_{\text{IDM}} + a_{\text{ff}}$
else
  $a \leftarrow \text{IDM}(v, \ell,\ T = T_{\text{human}} = 1.4\ \text{s})$
end if

C. Lateral Dynamics: MOBIL Lane-Change Model

In multi-lane scenarios, lane changes are governed by the MOBIL model [1]. A vehicle executes a lane change if both the safety and incentive criteria are satisfied. The safety criterion ensures that the new follower's required deceleration $\tilde{a}_n$ does not exceed a safe limit b_{safe}.

$$\tilde{a}_n \geq -b_{\text{safe}} \tag{3}$$

The incentive criterion requires that the lane-changing vehicle's net acceleration gain outweigh the disruption imposed on surrounding vehicles, discounted by a politeness factor [1], [25]:

$$\underbrace{\tilde{a}_c - a_c}_{\text{ego gain}} + p\underbrace{(\tilde{a}_n - a_n + \tilde{a}_o - a_o)}_{\text{others' change}} > \Delta a_{\text{th}} \tag{4}$$

D. Experimental Setup and Multi-Seed

The simulation environment is a circular ring road with a circumference of 791 meters and no entry or exit ramps, thereby eliminating potential boundary effects that could confound phantom-jam dynamics. Vehicle density is held constant at $\sim$44.2 veh/km per lane across all lane configurations (35 vehicles/lane: 34 background vehicles plus one designated perturber), ensuring that any observed differences between lane counts are attributable to lateral dynamics rather than a diluted road load [15].

The perturbation is triggered at $t = 30$ s: the perturber vehicle (vehicle ID 201) is forced to brake to 0 m/s via an instantaneous parameter override. Normal IDM parameters are restored at $t = 35$ s. The simulation then runs for 465 s post-perturbation, providing sufficient time to observe both jam propagation and eventual recovery. Key measured metrics are (i) mean speed $\bar{v}(t)$, (ii) speed standard deviation $\sigma_v(t)$ as a flow-stability proxy, and (iii) fraction of vehicles below 5 m/s (18 km/h) as a congestion proxy.

CACC vehicles are placed randomly among the background vehicles for each penetration rate. To mitigate AV-placement bias, three independent seed runs are performed per configuration. The AV placement seed for run index r is:

$$\text{seed}_{\text{AV}}(f_{\text{AV}}, r) = \lfloor f_{\text{AV}} \times 1000 \rfloor + r \times 1000, \quad r \in \{0, 1, 2\} \tag{5}$$

and the corresponding JavaScript simulation seed is $42 + 100r$. Reported metrics are the element-wise mean across all three runs; figures show shaded $\pm 1\sigma$ bands where applicable. Algorithm 2 summarizes the randomized placement procedure.

Algorithm 2 Randomized CACC Vehicle Placement

Require: penetration fraction f_{AV}, background count n, run index r
seed $\leftarrow \lfloor f_{\text{AV}} \times 1000 \rfloor + r \times 1000$
rng $\leftarrow$ Random(seed)
idx $\leftarrow$ shuffle($[0 \ldots n-1]$, rng)
$n_{\text{AV}} \leftarrow \text{round}(f_{\text{AV}} \times n)$
return idx$[0 \ldots n_{\text{AV}} - 1]$

In total, 132 simulation scenarios were executed: 3 seeds $\times$ 4 lane counts $\times$ 11 penetration rates (0%, 10%, ..., 100%).

III. RESULTS

Simulation results demonstrate that CACC systems are effective in mitigating phantom traffic jams and improving overall traffic flow. Subsequent sections analyze the effects of varying CACC penetration rates and compare performance across different lane configurations.

A. Baseline Phantom Jam Mitigation (Single Lane)

The single-lane ring road provides the clearest signal of CACC effectiveness because all vehicles must follow the vehicle immediately ahead with no lateral escape. Figure 1 shows vehicle trajectory heatmaps for six representative CACC penetration rates on the single-lane configuration. Each scatter point represents the position and speed of a vehicle at a given time step; data from all three seed runs are combined, thereby tripling the scatter density and yielding a more representative picture of ensemble behavior.

As shown in the vehicle trajectory plots of Fig. 1, at 0% CACC penetration, the stop-and-go waves are clearly visible with the circulating diagonal bands of red and orange for the entire 500 s simulation after the perturbation at $t = 30$ s. As shown in Fig. 1, the stop-and-go pattern continues until about 60% CACC. At 60% and 80% CACC penetration, the wave pattern is dramatically mitigated but not entirely gone. At 100% CACC, the trajectories are nearly uniform and green, which shows that cars are in free flow after the initial perturbation.

The traffic flow metrics in Fig. 2 show three metrics being measured: average speed, speed standard deviation,

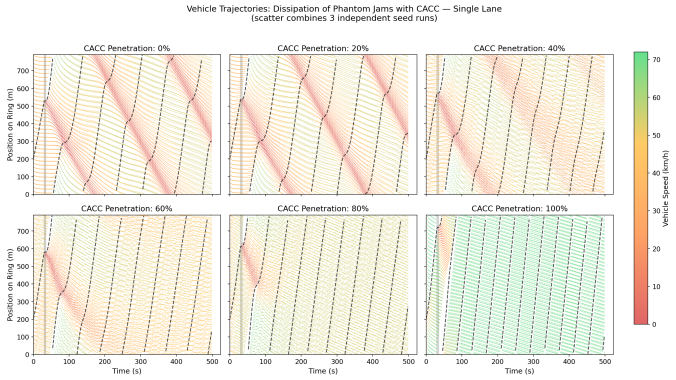

Fig. 1. Vehicle trajectory heatmaps showing phantom jam dissipation with increasing CACC penetration on a single-lane ring road. Color encodes vehicle speed from stopped (red) to free-flow (green).

and congestion (speed $< 18km/h$). The top graph shows the average vehicle speed after perturbation. Lower CACC penetrations (0% - 50% - solid lines) take longer to recover post-perturbation, whereas the dotted lines (60% - 100%) generally recover more quickly and also have higher average speeds. The speed standard deviation measures flow stability, and after the perturbation, all CACC levels increase sharply. Still, none of the solid lines recover, whereas the dotted lines eventually recover to a $0km/h$ deviation. Most strikingly, the fraction of vehicles traveling at $18km/h$ or below is a direct proxy for congestion. Only 40% - 100% CACC penetration rate scenarios recover from congestion, whereas 0% - 30% CACC penetration rate scenarios stabilize at approximately 0.25 under human-driven conditions.

These results confirm that CACC functions as a traffic shock absorber, significantly reducing phantom jams at penetration rates of 40% or higher [5], [24].

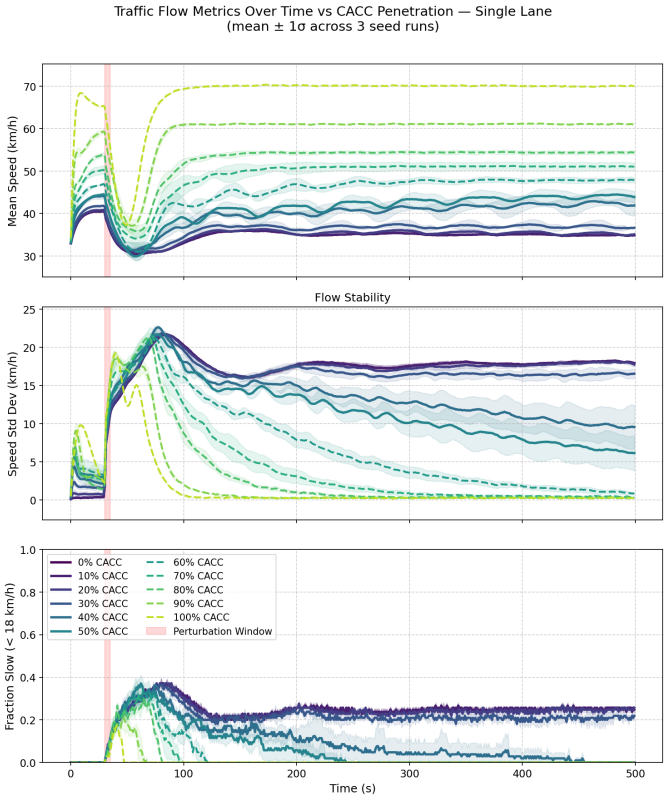

Fig. 2. Traffic flow metrics over time, single-lane scenario, 0%–100% CACC penetration. *Top:* Per-frame mean speed across all non-perturber vehicles. *Middle:* Speed standard deviation (flow stability; lower is more uniform). *Bottom:* Fraction of vehicles below 18 km/h (congestion proxy). Solid lines: 0%–50% CACC; dashed: 60%–100%. Shaded bands show $\pm 1\sigma$ across three seed runs. Perturbation window (30–35s) shaded red.

B. Multi-Lane Traffic Metrics and Wave Dissipation

To test the effectiveness of CACC across realistic road geometries, the simulation was extended to include two-, three-, and four-lane configurations while keeping the vehicle density at approximately 44.2 veh/km per lane (70, 105, and 140 vehicles respectively). The trajectory plots for the double-lane, triple-lane, and quad-lane configurations are shown in Figs. 3, 4, and 5, respectively.

In the double-lane case (Fig. 6), lane-changing provides an additional mechanism for congestion relief: even at 0% CACC, vehicles in lane 1 can pass the forming jam behind the perturber, reducing the congestion fraction from $\sim$0.25 (single-lane) to $\sim$0.14. The mean speed and standard deviation metrics show trends qualitatively similar to those in single-lane conditions, but with more noise at moderate penetration rates; this is a consequence of lane-change events perturbing the otherwise-coordinating CACC platoon strings. These findings are quite similar to Fig. 2, with no significant differences except that 100% CACC does not achieve the $0km/h$ speed standard deviation.

In the triple- and quad-lane cases (Figs. 7 and 8), additional lanes improve early flow; the reduction in friction and speed variance for slow vehicles is only 20%-40%, about half that

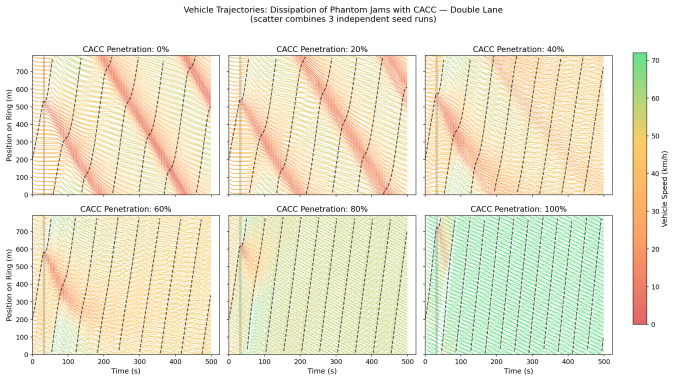

Fig. 3. Vehicle trajectory heatmaps: double-lane ring road (70 vehicles; 35 per lane, density 44.2 veh/km). Same color encoding as Fig. 1. The perturber is in lane 0; vehicles in lane 1 can bypass the forming jam.

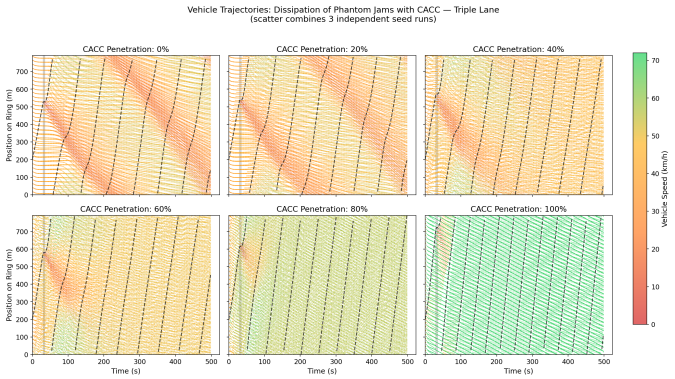

Fig. 4. Vehicle trajectory heatmaps: triple-lane ring road (105 vehicles; 35 per lane).

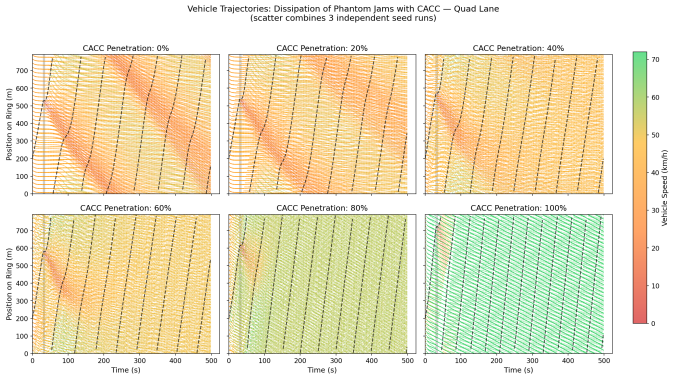

Fig. 5. Vehicle trajectory heatmaps: quad-lane ring road (140 vehicles; 35 per lane).

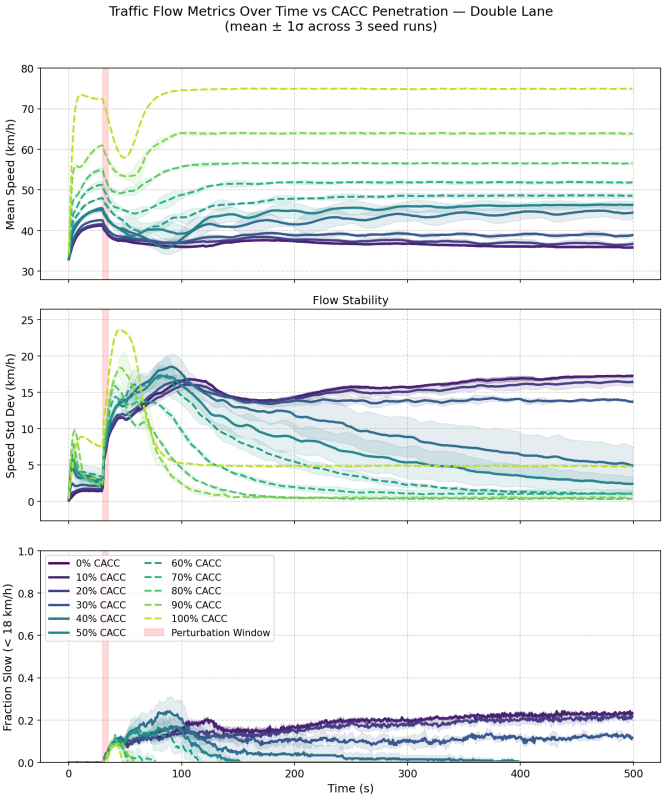

Fig. 6. Traffic flow metrics over time, double-lane scenario, 0%–100% CACC penetration. *Top:* Mean vehicle speed. *Middle:* Speed standard deviation (flow stability; lower is more uniform). *Bottom:* Congestion fraction (fraction of vehicles below 18 km/h). Solid lines: 0%–50%; dashed: 60%–100%. Shaded bands show $\pm 1\sigma$ across three seed runs. Lane switching reduces baseline congestion at 0% CACC to ≈0.14 vs. ≈0.25 single-lane, but at 100% CACC the standard deviation does not reach zero, reflecting residual lane-change noise.

on a single-lane road. In the tri- and quad-lane, after the perturbation window, the fraction of slow vehicles is nearly zero. This happens because other vehicles in other lanes can pass the slower traffic clusters without the clusters dissipating altogether. However, the speed standard deviation plots reveal a key trade-off: at 90%–100% CACC, multi-lane configurations exhibit a higher standard deviation than single-lane.

Increasing the number of lanes isn't always beneficial. When considering flow stability as measured by standard deviation (SD), multi-lane flow is much noisier at moderate penetration rates (30% - 60%) than single-lane flow. In the multi-lane stability curves in Figs. 7 and 8, there are wider oscillations that do not plateau even beyond $t = 200$s. Especially at 90% and 100% CACC penetration, the speed standard deviation spikes sharply and then returns to $0 km/h$, likely due to repeated lane changes. This confirms that, at higher CACC, additional lanes partially offset the benefits of the added communication.

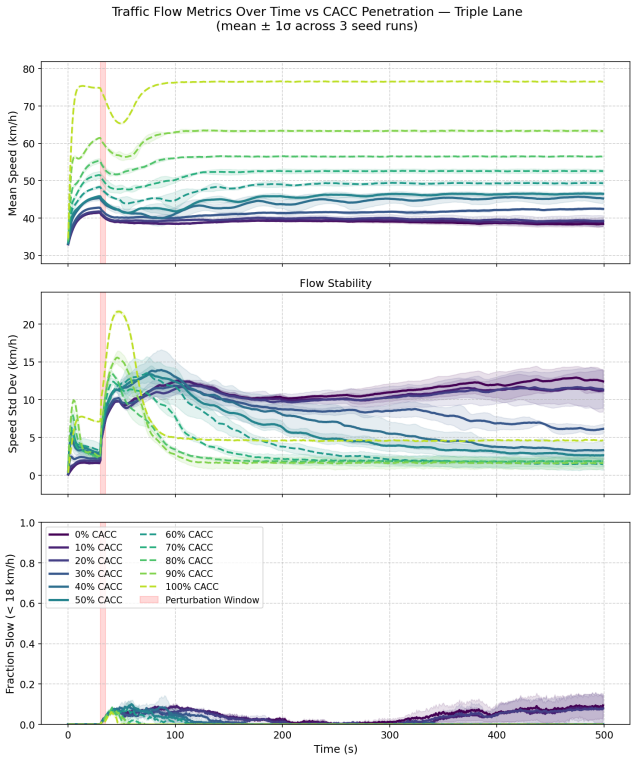

Fig. 7. Traffic flow metrics over time, triple-lane scenario, 0%–100% CACC penetration. Persistent speed standard deviation oscillations at 90%–100% CACC signal ongoing MOBIL-driven lane changes between otherwise-stable CACC platoon strings [9].

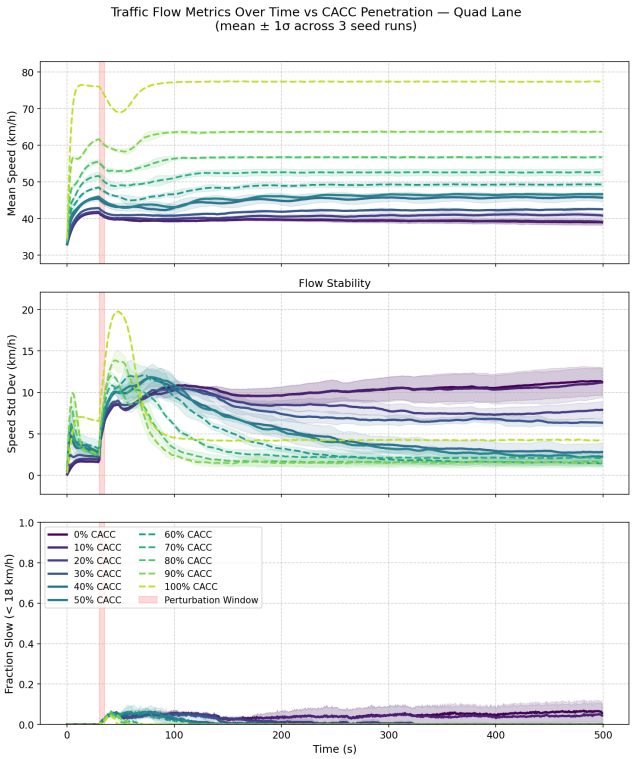

Fig. 8. Traffic flow metrics over time, quad-lane scenario, 0%–100% CACC penetration. Speed standard deviation oscillations at 90%–100% CACC are the most pronounced across all lane counts, confirming that additional lanes amplify MOBIL-induced instability at near-full CACC [1], [25].

C. Benefit of Lane Switching

To test the role of lane-switching in CACC control, per-lane speed, stability, and congestion were compared with the single-lane baseline in Fig. 9, which compares single-lane against double-, triple-, and quad-lane configurations.

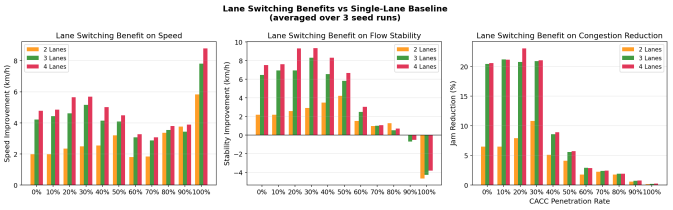

Fig. 9. Lane switching benefits relative to the single-lane baseline, averaged over three seed runs. *Left:* Speed improvement ($\Delta\bar{v}$ in km/h; positive = multi-lane faster). *Center:* Stability improvement ($\sigma_{SL} - \sigma_{ML}$ in km/h; positive = multi-lane more uniform; negative bars at 90%–100% CACC indicate MOBIL-induced instability). *Right:* Congestion reduction (positive = multi-lane less congested). Bars above zero (green) indicate multi-lane outperforms; bars below (red) indicate single-lane outperforms [7], [24].

As shown in the left graph in Fig. 9, lane switching is number of lanes and CACC level dependent. With 100% CACC, the four-lane configuration has an average speed improvement of 8.6 km/h over the single-lane configuration. While the two-lane configuration adds about 5.8 km/h to this, it demonstrates that higher CACC penetration with more lanes gives a higher speed improvement because cars can pass slower ones without the shock waves caused by human-driven cars.

The center panel reveals a reversal in stability: at 100% CACC penetration, *all* multi-lane configurations perform worse than single-lane, with stability improvements becoming negative (double-lane: -1.31 km/h; triple-lane: -1.20 km/h; quad-lane: -1.07 km/h in speed standard deviation). This occurs because, at near-full CACC penetration, the single-lane configuration achieves near-perfect string stability through longitudinal coordination alone, and the speed standard deviation approaches zero within 100 s of the perturbation. In multi-lane configurations, however, the MOBIL incentive criterion (Eq. 4) continues to trigger lane changes based on marginal speed differentials, even when the flow is already near-stable. Each lane change requires the new follower to adjust its headway to its new leader, creating a brief speed discontinuity. With a low politeness factor $p = 0.1$, these changes are frequent enough to sustain measurable speed oscillations. This is an important operational finding: at high CACC penetration rates, lane-change restrictions (e.g., platooning in dedicated lanes [13], [15]) may be preferable to open lane-changing, as the coordination overhead of MOBIL-triggered disruptions outweighs the lateral bypass benefit.

The right panel shows that at low CACC penetration (0% - 30%), congestion is reduced by $20\% - 24\%$ with 3-4 lanes relative to single lanes. Whereas in moderate CACC penetration (40% - 50%), the congestion-reduction benefits drop to around 5%. At extremely high CACC penetration levels, adding more lanes provides negligible benefit.

D. Quantitative Summary

Table II presents post-perturbation mean speed and congestion fraction for all configurations, averaged over three seed runs. The critical penetration thresholds for 50% and 90% jam reduction relative to the 0% CACC baseline are listed at the bottom.

TABLE II
POST-PERTURBATION METRICS (MEAN OVER THREE SEED RUNS, $t \geq 35$ S). SL = SINGLE LANE; DL = DOUBLE LANE; TL = TRIPLE LANE; QL = QUAD LANE. MEAN SPEED IN M/S; CONGESTION FRACTION = FRACTION OF VEHICLES BELOW 5 M/S. CRITICAL PENETRATION THRESHOLDS FOR 50% AND 90% JAM FRACTION REDUCTION RELATIVE TO 0% CACC BASELINE SHOWN AT BOTTOM.

CACC	Mean Speed (m/s)				Congestion Fraction			
(%)	SL	DL	TL	QL	SL	DL	TL	QL
0	9.61	10.16	10.78	10.94	0.252	0.187	0.048	0.046
20	9.71	10.37	11.00	11.28	0.246	0.166	0.038	0.015
40	11.10	11.80	12.24	12.49	0.097	0.046	0.011	0.008
60	12.58	13.08	13.43	13.49	0.035	0.018	0.006	0.007
80	14.59	15.53	15.58	15.65	0.021	0.003	0.002	0.001
100	18.90	20.54	21.09	21.36	0.003	0.002	0.001	0.001
50% jam reduction threshold: SL = 40%, DL = 40%, TL = 30%, QL = 20%								
90% jam reduction threshold: SL = 70%, DL = 60%, TL = 70%, QL = 70%								

In addition to this tabular summary, a unified comparison across all lane configurations is presented in Fig. 10.

Fig. 10. Phantom jam mitigation comparison across lane configurations. Top row: absolute metrics. Lower rows: improvement of each multi-lane configuration relative to the single-lane baseline.

Multi-lane configurations consistently outperform the single-lane baseline in all three studies and all CACC penetration levels. The mean speed advantage after perturbation on multi-lane roads varies across $0\% - 100\%$ CACC, with four lanes and full penetration reaching over $72 km/h$, vs single-lane full penetration reaching $64 km/h$. The speed advantage increases exponentially with CACC penetration.

On the other hand, the flow stability comparisons show that, for high CACC penetration, the speed standard deviation for all

configurations is lower at $5.4km/h$ when measured at $70\% - 80\%$. In each flow stability graph comparing two, triple, and quad vs. single, $90\% - 100\%$ CACC causes stability to drop by $5.4km/h$.

Now, comparing congestion, we see it reduced by more than 20% over single-lane traffic, up to $50\% - 60\%$ at *CACC* penetration. Three- and four-lane configurations reduce the jam fraction by more than 20 percentage points compared to single-lane configurations. As CACC penetration rises above 60% all, lane configurations decrease towards zero. These results indicate that when CACC penetration is low or moderate (below 60%), multi-lane roads provide a substantial benefit in reducing congestion by at least 20%. And the CACC deployment alone is sufficient to eliminate phantom jams regardless of lane count and full CACC penetration.

IV. Conclusion

This study quantified the impact of CACC penetration on phantom traffic jam formation through a density-preserving microsimulation sweep of 132 configurations (3 seeds $\times$ 4 lane counts $\times$ 11 penetration rates). The following are the three key findings:

A CACC penetration of 40%–60% suppresses phantom jams regardless of lane count. On the other hand, when below 40%, stop-and-go waves persist indefinitely; above 60%, the traffic flow recovers to free flow within 60–120 s across all configurations. As the simulation ran for 500 seconds, it is unlikely that, in the current intentional configuration, the stop-and-go wave would end. This threshold is consistent with the nonlinear-stability analysis of Molnar and Orosz [5] and is slightly below the $\sim$50% single-lane estimate of Shladover et al. [8], likely because the density-preserving multi-lane setup provides additional lateral absorption capacity.

Lane switching provides 20%–24% congestion relief at 0%-30% CACC but becomes counterproductive to flow stability above 80% CACC. The MOBIL incentive criterion, with politeness factor $p = 0.1$, continued to trigger lane changes based on marginal speed differentials even when CACC longitudinal coordination has already stabilized the flow, sustaining measurable speed oscillations; dedicated CACC lane policies [13], [15] or higher politeness factors [25] should therefore be considered at high penetration rates.

Investing in CACC V2X infrastructure should be prioritized over road-widening once penetration exceeds 40%: additional lanes deliver diminishing congestion-reduction returns above 60% CACC, while CACC alone eliminates phantom jams at full penetration regardless of lane count. This provides the Department of Transportation planners a concrete 40% market penetration target achievable through regulatory incentives and fleet mandates [8], [21].

Limitations and future work

The ring-road topology isolates phantom-jam dynamics but excludes on-ramp merging, lane drops, and signalized intersections. Extending to heterogeneous populations (e.g., aggressive or distracted drivers [19]) may shift the critical threshold. Future work should validate the 40%–60% threshold against real-world mixed-traffic data [20] and explore optimal CACC platoon sizing [14], [17] and string-stability controller design [11], [12], [18], [23] for the high-penetration regime where MOBIL-induced instability is most pronounced.

Acknowledgment

We thank Dr. Josh Siegel, Assistant Professor of Computer Science and Engineering at Michigan State University, for valuable feedback and guidance throughout this research. We acknowledge the open-source `traffic-simulation-de` simulator by Martin Treiber, upon which this study was built, and the comprehensive prior art by Treiber, Shladover, Molnar, and collaborators that shaped the experimental design.

Credit Authorship Contribution Statement

Aashish Harishchandre: Designed and implemented the full simulation logging feature, including the event writer, per-frame data collection, JSON log export, and the scenario-logging UI panel for browser-side data capture. Extracted and interpreted post-simulation metrics from collected logs. Data Validation: Reviewed and interpreted collected data. Writing: Review and Editing.

Lucas Wolstencroft: Formulated the density-preserving multi-lane sweep study design and identified the phantom-jam suppression research question. Selected IDM/MOBIL as the modeling framework, derived CACC parameter values (reduced time headway, feedforward gain), and specified the ring-road perturbation scenarios. Implemented the foundational CACC vehicle model and early run testing. Writing: Review and Editing.

Prabhaav Ravikumar Pillai: Implemented the JSON-driven Scenario Manager engine, enabling scenario specification and programmatic vehicle control; implemented the vehicle platooning feature and lane-change disable capability; built the Python/Playwright multi-seed simulation pipeline that executed the full scenario sweep. Data Visualization: produced all figures for the paper. Writing: Review and Editing.

References

[1] A. Kesting, M. Treiber, and D. Helbing, "General lane-changing model MOBIL for car-following models," *Transp. Res. Rec.*, vol. 1999, no. 1, pp. 86–94, Jan. 2007, doi: 10.3141/1999-10.

[2] X. Song, Z. Dong, F. Ding, and W. Lu, "Data-iteration cooperative adaptive cruise control of mixed heterogeneous vehicle platoons with unknown dynamic characteristics," *Asian J. Control*, vol. 25, no. 4, pp. 2776–2789, Nov. 2022, doi: 10.1002/asjc.2975.

[3] H. Wang, X. Li, X. Zhang, J. Hu, X. Yan, and Y. Feng, "Cut through traffic like a snake: Cooperative adaptive cruise control with successive platoon lane-change capability," *J. Intell. Transp. Syst.*, pp. 1–22, Aug. 2022, doi: 10.1080/15472450.2022.2114081.

[4] M. Razzaghpour, R. Valiente, M. Zaman, and Y. P. Fallah, "Predictive model-based and control-aware communication strategies for cooperative adaptive cruise control," *IEEE Open J. Intell. Transp. Syst.*, vol. 4, pp. 232–243, 2023, doi: 10.1109/OJITS.2023.3259283.

[5] T. G. Molnar and G. Orosz, "Destroying phantom jams with connectivity and automation: Nonlinear dynamics and control of mixed traffic," *Transp. Sci.*, vol. 58, no. 6, pp. 1319–1334, Jul. 2024, doi: 10.1287/trsc.2023.0498.

[6] M. Guériau and I. Dusparic, "Quantifying the impact of connected and autonomous vehicles on traffic efficiency and safety in mixed traffic," in *Proc. IEEE Intell. Transp. Syst. Conf. (ITSC)*, Sep. 2020, doi: 10.1109/ITSC45102.2020.9294174.

[7] B. van Arem, C. J. G. van Driel, and R. Visser, "The impact of cooperative adaptive cruise control on traffic-flow characteristics," *IEEE Trans. Intell. Transp. Syst.*, vol. 7, no. 4, pp. 429–436, Dec. 2006, doi: 10.1109/TITS.2006.884615.

[8] S. E. Shladover, D. Su, and X.-Y. Lu, "Impacts of cooperative adaptive cruise control on freeway traffic flow," *Transp. Res. Rec.*, vol. 2324, no. 1, pp. 63–70, Jan. 2012, doi: 10.3141/2324-08.

[9] T. Zong, Y. Li, and Y. Qin, "Enhancing stability of traffic flow mixed with connected automated vehicles via enabling partial regular vehicles with vehicle-to-vehicle communication function," *Physica A*, vol. 641, p. 129750, May 2024, doi: 10.1016/j.physa.2024.129750.

[10] J. Wang, L. Lu, and S. Peeta, "Real-time deployable and robust cooperative control strategy for a platoon of connected and autonomous vehicles by factoring uncertain vehicle dynamics," *Transp. Res. Part B*, vol. 163, pp. 88–118, Sep. 2022, doi: 10.1016/j.trb.2022.06.012.

[11] X. Yue, H. Shi, Y. Zhou, and Z. Li, "Hybrid car following control for CAVs: Integrating linear feedback and deep reinforcement learning to stabilize mixed traffic," *Transp. Res. Part C*, vol. 167, p. 104773, Oct. 2024, doi: 10.1016/j.trc.2024.104773.

[12] Y. Zhou, S. Ahn, M. Wang, and S. Hoogendoorn, "Stabilizing mixed vehicular platoons with connected automated vehicles: An H-infinity approach," *Transp. Res. Procedia*, vol. 38, pp. 441–461, 2019, doi: 10.1016/j.trpro.2019.05.024.

[13] E. Doğan and E. Korkmaz, "Performance and safety assessment of dedicated lane for connected automated vehicles," *Int. J. Intell. Transp. Syst. Res.*, Jan. 2026, doi: 10.1007/s13177-025-00602-9.

[14] J. Zhou and F. Zhu, "Analytical analysis of the effect of maximum platoon size of connected and automated vehicles," *Transp. Res. Part C*, vol. 122, p. 102882, Jan. 2021, doi: 10.1016/j.trc.2020.102882.

[15] M. Amirgholy, M. Shahabi, and H. O. Gao, "Traffic automation and lane management for communicant, autonomous, and human-driven vehicles," *Transp. Res. Part C*, vol. 111, pp. 477–495, Feb. 2020, doi: 10.1016/j.trc.2019.12.009.

[16] H. Köroğlu, "String-stable cooperative adaptive cruise control with minimized time headway in the face of delayed communication," *IEEE Control Syst. Lett.*, vol. 8, pp. 400–405, 2024, doi: 10.1109/LCSYS.2024.3392716.

[17] M. S. Salek, M. B. Thakur, K. Ala, M. Chowdhury, and V. Krovi, "An overview of automated vehicle longitudinal platoon formation strategies," *ACM J. Auton. Transp. Syst.*, May 2025, doi: 10.1145/3736642.

[18] K. Liu, P. Jiao, W. Hong, and Y. Chen, "Bilateral control model for autonomous vehicles based on deep reinforcement learning," *IEEE Trans. Intell. Transp. Syst.*, vol. 26, no. 5, pp. 6216–6230, May 2025, doi: 10.1109/TITS.2025.3548481.

[19] M. Treiber and A. Kesting, *Traffic Flow Dynamics: Data, Models and Simulation*. Berlin, Germany: Springer, 2013, doi: 10.1007/978-3-642-32460-4.

[20] C. G. Park *et al.*, "Implementation of a V2V platooning testbed: Performance comparison of CACC vs. ACC," Oct. 2025, doi: 10.1109/ICCE-ASIA67487.2025.11263572.

[21] R. Korbmacher *et al.*, "Emergent cooperative driving strategies for stop-and-go wave mitigation via multi-agent reinforcement learning," arXiv, 2025, doi: 10.48550/arXiv.2511.14378.

[22] M. Treiber, A. Hennecke, and D. Helbing, "Congested traffic states in empirical observations and microscopic simulations," *Phys. Rev. E*, vol. 62, no. 2, pp. 1805–1824, Aug. 2000, doi: 10.1103/PhysRevE.62.1805.

[23] K. Liu *et al.*, "Enhancing mixed traffic stability with TD3-driven bilateral control in autonomous vehicle chains," *Sustainability*, vol. 17, no. 11, 2025, doi: 10.3390/su17114790.

[24] M. Di Vaio *et al.*, "Cooperative shock waves mitigation in mixed traffic flow environment," *IEEE Trans. Intell. Transp. Syst.*, vol. 20, no. 12, pp. 4339–4353, Dec. 2019, doi: 10.1109/TITS.2018.2883485.

[25] J. He *et al.*, "Enhancing traffic safety and efficiency with GOLC: A global optimal lane-changing model integrating real-time impact prediction," *Technologies*, vol. 13, no. 9, 2025, doi: 10.3390/technologies13090410.

[26] J. Lioris *et al.*, "Platoons of connected vehicles can double throughput in urban roads," *Transp. Res. Part C*, vol. 77, pp. 292–305, Apr. 2017, doi: 10.1016/j.trc.2017.01.023.

[27] V. Milanés *et al.*, "Cooperative adaptive cruise control in real traffic situations," *IEEE Trans. Intell. Transp. Syst.*, vol. 15, no. 1, pp. 296–305, Feb. 2014, doi: 10.1109/TITS.2013.2278494.

[28] B. Liu and A. El Kamel, "V2X-based decentralized cooperative adaptive cruise control in the vicinity of intersections," *IEEE Trans. Intell. Transp. Syst.*, vol. 17, no. 3, pp. 644–658, Mar. 2016, doi: 10.1109/TITS.2015.2486140.

[29] A. Hegyi and S. P. Hoogendoorn, "Dynamic speed limit control to resolve shock waves on freeways—field test results of the SPECIALIST algorithm," Sep. 2010, doi: 10.1109/ITSC.2010.5624974.

[30] A. Hegyi *et al.*, "Towards a practical application of model predictive control to suppress shock waves on freeways," Jul. 2007, doi: 10.23919/ECC.2007.7069058.

[31] A. Hegyi, B. De Schutter, and J. Hellendoorn, "Optimal coordination of variable speed limits to suppress shock waves," *IEEE Trans. Intell. Transp. Syst.*, vol. 6, no. 1, pp. 102–112, Mar. 2005, doi: 10.1109/TITS.2004.842408.

[32] Y. Sugiyama *et al.*, "Traffic jams without bottlenecks—experimental evidence for the physical mechanism of the formation of a jam," *New J. Phys.*, vol. 10, no. 3, p. 033001, Mar. 2008, doi: 10.1088/1367-2630/10/3/033001.

[33] R. E. Stern *et al.*, "Dissipation of stop-and-go waves via control of autonomous vehicles: Field experiments," *Transp. Res. Part C*, vol. 89, pp. 205–221, Apr. 2018, doi: 10.1016/j.trc.2018.02.005.

[34] D. Schrank, B. Eisele, and T. Lomax, "2019 Urban Mobility Report," Texas A&M Transportation Institute, College Station, TX, Aug. 2019. [Online]. Available: https://static.tti.tamu.edu/tti.tamu.edu/documents/umr/archive/mobility-report-2019.pdf